Energy Storage Materials 75 (2025) 104003

Contents lists available at ScienceDirect

Energy Storage Materials

journal homepage: www.elsevier.com/locate/ensm

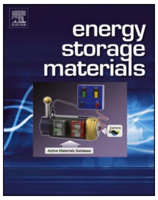

High power and energy density graphene phase change composite materials for efficient thermal management of Li-ion batteries

Chengqi Zhang [a], Yi Mao [a], Kaiwen Li [a], Yingjun Liu [a], Zhen Xu [a], Kai Pang [a,*], Shengying Cai [b,*], Liwu Fan [c,*], Chao Gao [a,*]

[a] *MOE Key Laboratory of Macromolecular Synthesis and Functionalization, Department of Polymer Science and Engineering, Key Laboratory of Adsorption and Separation Materials & Technologies of Zhejiang Province, Zhejiang University, 38 Zheda Road, Hangzhou 310027, China*
[b] *Center for Healthcare Materials, Shaoxing Institute, Zhejiang University, Shaoxing 312000, China*
[c] *Institute of Thermal Science and Power Systems, School of Energy Engineering, Zhejiang University, 38 Zheda Road, Hangzhou 310027, China*

ARTICLE INFO

Keywords:
Thermal conductivity
Hyperbolic graphene
Phase change material
Energy density
Power density

ABSTRACT

The safety concern of Li-ion battery cells, mainly caused by thermal runaway, has become a fundamental bottleneck that restricts their wider adoption in energy sector. Phase change material system is an available thermal management strategy to suppress the thermal runaway of batteries, however, the unresolved trade-off between high power and energy density greatly limits its practical applications. Here we present an efficient thermal management system with high power and energy density by hyperbolic graphene phase change material, preventing the rapid heat accumulation of Li-ion battery cells. This composite material consists of hyperbolic graphene framework and paraffin, exhibiting the overwhelming thermal conductivity of ~30.75 W/mK at 12.5 wt% graphene loading and ultrahigh retention (90 %) of latent heat, beyond than most of reported phase change composites. We demonstrate our paraffin-graphene composite (PGC) shows almost three-folds improvement of efficient energy density at high power density compared with commercial paraffin. The temperature of a battery pack in series at 3.75 C rate capability is <60℃ with protection of PGC system, far below ~120℃ of bare battery pack. Our PGC system expands the usability and safety of Li-ion batteries and provides a reliable battery thermal management strategy towards extreme fast-charging goals.

1. Introduction

Rechargeable batteries, especially Li-ion batteries (LIBs), have been put on the major stage of future energy system with the power sector transformation to renewables and the advancement of battery technologies. Since the commercialization of LIBs, their performance in diverse aspects, such as capacity, cycle life and charging rate, has improved significantly [1–3]. One of the primary remaining concerns is battery safety [4,5], which has caused many hazardous events in electric vehicles. Battery safety is related to the thermal management under overheating or overcharging conditions, whose failure temperature can move beyond their respective safety windows. In contrast to conventional thermal management systems (air, liquid and heat pipe cooling), phase change material (PCM) system can improve the safety of battery energy components by time shifting or reducing peak thermal loads, possessing the advantages of fast heat dissipation, high temperature uniformity, low cost and simple structure, which exhibited optimal overall performances [6].

The efficiency of PCM is defined by its effective energy and power density—the available heat storage capacity and the heat transport speed at which it can be accessed [7]. The intrinsically low thermal conductivity of PCMs limited the heat diffusion speed and seriously hindered the effective latent heat storage in practical applications [8]. Many efforts have been devoted to improving the thermal conductivity of PCMs by composite them with highly thermal conductive fillers, such as dispersing highly conductive nanoscale or micro-sized particles with PCMs, inserting a metallic and carbon fiber matrix and impregnating a porous graphite or graphene matrix into PCMs [9–11]. However, the fast thermal transport with higher power density was usually realized by the high mass loading of filler in PCM composites, dramatically reducing the total energy density due to the low phase change ingredients. For example, the thermal conductivity of PCMs can be up to 30 W/mK at graphite loading of 40 wt%, but the retention of latent heat was only 60 % compared with pure PCM [12]. There remains a great challenge to

---

* Corresponding authors.
E-mail addresses: pangkai2015@zju.edu.cn (K. Pang), shengyingcai@zju.edu.cn (S. Cai), liwufan@zju.edu.cn (L. Fan), chaogao@zju.edu.cn (C. Gao).

https://doi.org/10.1016/j.ensm.2025.104003
Received 26 October 2024; Received in revised form 21 December 2024; Accepted 2 January 2025

break the trade-off between high energy and power density in PCM composites.

Here we resolve the trade-off between high effective energy and power density, by adopting hyperbolic graphene framework as highly thermal conductive filler to fabricate optimal PCM composite. As-prepared paraffin-graphene composite (PGC) displays the record thermal conductivity of ~30.75 W/mK at 12.5 wt% filler loading and the high latent heat retention of 90 %, which were never been reached in existing PCMs. We further reveal the PGC exhibits the effective ultra-high energy density of 1003 Wh/kg with power density of 2927 W/kg, which was three times more than pure paraffin. We then apply it for passive thermal management system of commercial 14500 LIB cells and demonstrate the PGC significantly suppresses the thermal runaway of batteries at high rate capability of 3.75 C. The battery pack temperature always keeps the stable temperature at phase transition point of ~42℃ even at 10,000 charge-discharge cycles with protection of PGC cooling system, which was the safe and efficient operating temperature of LIBs.

2. Experimental section

2.1. Materials

Aqueous GO solution (2 wt%) with an average lateral size of 10–30 μm was purchased from Hangzhou Gaoxi Technology Co. Ltd. (www.gaoxitech.com). Other chemicals and reagents were supplied from Sinopharm Chemical Reagent Co., Ltd. (China).

2.2. Fabrication of hyperbolic graphene-paraffin composites for LIBs

2.2.1. Fabrication of hyperbolic graphene aerogels (HGAs)

The GO film was fabricated by casting method with room-temperature drying. As-obtained GO film was directly put into the hydrazine hydrate solution (30 wt%) to achieve the preparation of graphene oxide aerogels by hydroplastic foaming method. Subsequently, the graphene oxide aerogels were conducted with chemical reduction (HI/HAc vapor) and high-temperature graphitization (3150℃) to restore the graphene structure and obtain HGAs. The detailed high-temperature graphitization process was divided into three steps: heating rate of 2℃/min below 1600℃, heating rate of 10℃/min from 1600 to 3150℃, and keeping for 30 min at 3150℃.

2.2.2. Vacuum infusion of paraffin into HGA

The phase-change paraffin with transition point of 42℃ was purchased from Dongguan Xinsheng Plastic Technology Co., LTD. Before vacuum infusion, the paraffin was melted at 60℃ to ensure the excellent liquidity. Then, the HGA monolith was soaked into the liquid paraffin, and vacuumized at pressure of 10 Pa for 2 h The paraffin-graphene composite (PGC) was obtained after cooling to room temperature.

2.2.3. Manufacturing of PGCs for LIB thermal management system

A stack of PGC monoliths was performed with hot-press molding, and tailored into the specific shape to achieve the embedding of LIB cell pack. To eliminate the thermal contact resistance between individual battery and PGC monolith, every LIB was inserted into the phase-change materials in softening state of paraffin. The polyimide film was used as insulation layer to avoid the short circuit of batteries and the nickel foils was adopted to connect the different cell by hot welding.

2.2.4. PCM materials testing device for energy density and power density

The total power of the heating chip (1 × 1 cm^2, Alumina ceramic chip) was adjusted by an auto-ranging DC power supply (ITECH IT6522D). The thermal silicone grease (ShinEtsu) was applied to both the thermal insulation foam (Polycarbonate foam, Covestro) and the heating chip surface with the PGC centered on the chip. Then, the heating chip was fixed on the thermal insulation foam and the thermal insulation around PGC was composed of the thermal insulation foam. A type-K thermocouple (TT-K-30, Maxomega) was embedded in the heating surface to measure the surface temperature.

Due to the thermal insulation foam sealed around the PGC, the heat loss was deemed negligible. The power density (P) and effective energy density (E) was calculated as follows. The m was the mass of PCM. The product of voltage (U) and current (I) was the input power. The high thermal resistance presented a fundamental limitation on the maximum achievable time-dependent power density of PCM thermal management. When the temperature of PCM researched phase change point, the PCM was not always fully melted, thus defining the effective time (t).

$$P = \frac{U \times I}{m}$$

$$E = \frac{U \times I \times t}{m}$$

2.3. Characterizations

The morphology and microstructure of HGA were characterized by field-emission SEM (Hitachi S4800) and TEM (FEI Titan G2 60–300). Raman measurements were performed on a Renishaw in Via-Reflex using a 532 nm laser beam. XRD patterns was measured with a X-pert Powder diffractometer. The thermal conductivity was measured by laser thermal conductivity testing instrument (NETZSCH LFA467). The specific heat capacity (Cp) and latent heat were measured by DSC (TA Q200) at a heating rate of 10℃/min under nitrogen atmosphere. The IR thermal photos were captured by a high-resolution infrared imager (FLIR T630sc). The temperature acquisition system (MT500P, Shenhua Electronic Technology) was adopted to achieve the real-time temperature detection of battery pack with K-type thermocouples. The electrical properties of HGA were measured by the Keithley-2400 Source Meter using the four-wires method. The conductivity was calculated according to the equation $\sigma_e = l/(R \times S)$, where l, S and R are the length and the cross-sectional area and electrical resistance of the HGA, respectively. The tensile measurements were performed on the Instron Legend 2344 machine.

The galvanostatic cycling measurements of individual LIB cell at different temperatures (in a constant temperature chamber) were carried out on a Land BT2000 battery test system. The battery pack was assembled by inserting 16 (4 × 4) 14500 LIBs into pre-punched PCMs and then connected in parallel through 100 μm thick nickel foil. The bare battery pack was prepared by directly connecting 16 (4 × 4) 14500 LIBs in parallel with the same size. In order to detect battery temperature during tests, thermocouple probes were pasted to the battery surface by tapes. The capacity rate and voltage range employed for battery pack tests were 2.75–3.75 C and 2.75–4.3 V, respectively. Battery packs connected with temperature sensors were tested by a Land CT6002A.

3. Results and discussion

3.1. Thermal runaway mechanism and PGC thermal management system

Thermal runaway of LIB cells is referred to a chain reaction [13,14] by various incentives such as short circuit, fast charge or discharge rate and mechanical shocks, which can emit large amounts of heat and harmful gases and caused the battery to catch fire and explode. The evolution of this phenomenon is divided into three stages: self-extinguish with no obvious heat, heat accumulation with obvious heat and unstoppable battery burning with mass heat (Fig. 1a). Owing to the irreversible character of thermal runaway, the efficient thermal management should be adopted to avoid the break in the balance of heat generation and dissipation at stage I, and preventing the occurrence of stage II and III.

We exhibited a typical case of thermal runaway of LIB pack with 16 individual 14500 cells in series (Fig. 1b and c), which operated at fast

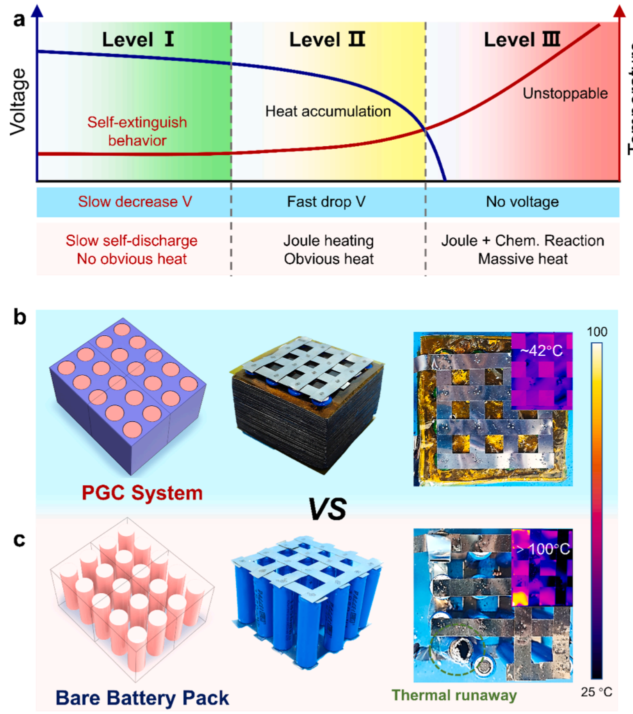

Fig. 1. PGC thermal management system for LIB cells. **(a)** The three stages during thermal runaway of LIB cells. **(b)** Illustration for battery pack with PGC cooling system and its corresponding digital photo and thermal imaging during charging-discharging cycles at 30 A. **(c)** Illustration for bare battery pack and its corresponding digital photo and thermal imaging during charging-discharging cycles at 30 A.

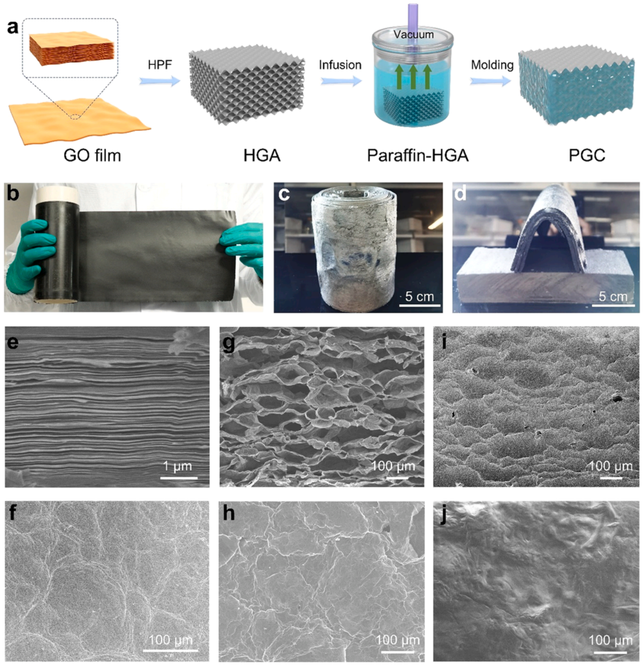

Fig. 2. Fabrication and characteristic of PGC materials. **(a)** Representative diagram of the fabrication of PGC. **(b)** A roll of GO film, and **(c)** HGA with length of ~200 cm and width of ~13 cm. **(d)** Large, flat PGC monolith and arch-shaped PGC monolith. The cross-sectional SEM images of **(e)** GO film, **(g)** HGA and **(i)** PGC. The surface SEM images of **(f)** GO film, **(h)** HGA and **(j)** PGC.

charge or discharge rate of 30 A. There was an obvious thermal runaway phenomenon in battery cells with local temperature over 100℃ and exploding, resulting in the fracture of solder joints and lots of white smoke. As comparison, a PCM cooling system of LIBs was built by inserting the battery pack into the PGC monolith, and adopting polyimide film as insulted layer to avoid the short circuit between graphene and cell connectors (Fig. 1b). We demonstrated the PGC system avoided the thermal runaway and efficiently suppressed the temperature rise of batteries under the same working conditions, which only reached the temperature of 40℃. We performed the capacity retention test at different temperature for individual 14500 cell with 500 cycles (Figure S1). This revealed that ~40℃ was an optimal temperature of battery to maintain a high capacity retention (> 70 %) as like as room temperature (25℃). Those results indicate the efficient thermal management system of PGC material was essential to realize the long life and security of LIBs.

3.2. *Hyperbolic graphene aerogel -based phase change materials*

The PGC was composed with hyperbolic graphene aerogel (HGA) framework and phase change paraffin (Fig. 2a). The HGA was fabricated by hydroplastic foaming (HPF) method according to our previous reported works [15–17]. After foaming of graphene oxide (GO), the chemical reduction and high-temperature graphitization were performed to restore the perfect crystal structure of graphene [18]. Due to the mature technology of roll-to-roll casting, a raw material of continuous GO film (Fig. 2b) was easily adopted to fabricate rolled hyperbolic graphene aerogel (HGA) with a length of ~200 cm and a width of ~13 cm (Fig. 2c). Then the HGA was soaked into the liquid paraffin (60℃) to achieve PGC material with vacuum infusion. The HGA demonstrated adequate structural integrity during the vacuum infusion process (Figure S2), and under negative pressure, the liquid paraffin was easily pushed into the open pores of HGA. Finally, the formed PGC was achieved when the paraffin cooled to room temperature. The large PGC monolith was easily tailored or machined into various shapes because of the softening feature of paraffin (Fig. 2d), meeting the diversified demands in the thermal management of cylindrical, pouch and prismatic battery.

The microstructure evolution during the preparation of PGC was illustrated in Fig. 2e-j. The lamellar GO film was stacked by GO nanosheets (Fig. 2e) with interlayer spacing of ~ 1 nm, which was proved by its XRD diffraction peak (001) at ~ 10° (Figure S3a). There were many oxygen-containing groups on the surface and edge of GO sheet, which resulted the obvious D peak (~ 1350 cm^{-1}) in Raman spectrum (Figure S3b). We observed some wrinkles spread on the dense surface of GO film (Fig. 2f) due to the strong solvent surface tension during the drying from GO suspension. After HPF process, many open pores were generated between the interlayer of GO sheets (Fig. 2g), forming the porous aerogels with hyperbolic structure. The surface morphology of HGA also exhibited the dense structure with more small wrinkles (Fig. 2h), indicating the pores only existed along the in-plane direction without disrupting the highly orientated graphene structure along the out-of-plane direction. After chemical reduction and high-temperature graphitization, the graphene oxide sheets restored the high crystalline quality of the graphite lattice and exhibited negligible structural defects, as confirmed by the long-range crystalline order in HR-TEM inspection (Figure S4). The XRD diffraction peak of (002) and 2D Raman peak were appeared at ~ 26° and ~ 2620 cm^{-1}, respectively (Figure S3), further corroborated the nearly complete restoration of graphene in HGA [18]. Furthermore, the cross-section and surface images of PGC demonstrated the infiltration of paraffin did not disturb the seamlessly connected hyperbolic graphene sheets of HGA framework (Fig. 2i and j), which was the precondition for the highly thermal conductivity of its composites.

3.3. *Thermal properties and phase change storage of PGC*

The thermal management ability of the PCM is depended on the thermal properties of PGC, such as thermal conductivity, the solid-liquid phase transition behavior, and loading capacity of paraffin [7]. The thermal conductivity (λ) of PGC increased from 6.7 to 82.4 W/mK with graphene content (ω) from 2.26 to 30 wt% (Fig. 3a and S5), scaling as an exponential relation of $\lambda \sim \omega^{0.96}$. The thermal enhancement factor $(\lambda_{PGC}-\lambda_{paraffin})/\lambda_{paraffin}/\omega)$ of PGC was up to ~ 590 at graphene loading of 2.26 wt%, surpassing the most of reported phase change composites [10,12,19–22]. We compared the thermal conductivity with other thermally conductive composites (Table S1), exhibiting the superior phonon transport characteristic of our PGC material [23–26]. The phase transition behavior was investigated by DSC measurements. As shown in Fig. 3b, the peak of melting temperature had subtly decrease with the adding of graphene, changed from 46.5℃ (2.26 wt% filler) to 44℃ (30 wt% filler). This can be attributed to the rapidly thermal transport network at high graphene loading, which accelerated the melting process of paraffin. The phase-change latent heat is correlated to the loading of paraffin in the PGCs, which can be calculated on the enclosed area inside the melting peak of DSC curves. We demonstrated the latent heat was up to 200 J/g even with the graphene loading of 12.5 wt%, which only exhibited the loss of 9.1 % than pure paraffin (Fig. 3c). In the meanwhile, the specific heat of PGC was also up to 1.92 J/gK, exhibiting a high retention rate of 88.7 %. We further compared the thermal conductivity versus latent heat retention of PGCs with other reported PCM composites (Fig. 3d). Owing to the high-efficient thermal enhancement at low graphene content (12.5 wt% filler), the PGC achieved superior thermal conductivity and high latent heat retention, enabling it to maintain the battery within a stable temperature range an exhibiting the overwhelming superiority over existing PCM systems [12,20–22, 27–35]. Those characteristics enabled the PGC systems to display higher efficiency, a simpler structure and lower weight compared to other thermal management systems [35,36] (Table S2).

As an optimally thermal and electrical filler network of HGA, the obtained PGCs also possessed the high electrical conductivity (σ). The highest σ of PGC was over 10^5 S/m when graphene content >18.8 wt% (Fig. 3e), conforming with the relation of $\sigma \sim \omega^{1.22}$, which was greater than the carbon- or metal- based PCM composites [9,37,38]. The outstanding electrical transport ability of PGC can be attributed to the hyperbolic network formed by face-to-face contact of 2D sheets [16], which provides the potential for rapid electric heating, thereby preventing thermal management failure in extreme cold environments. We gave the temperature plots of PGC during the electric heating process at electric current density from 0.25 to 0.75 A/cm^2 (Fig. 3f). We demonstrated the PGC not only achieved the ultra-fast heat generation from room temperature to 30℃ within 10 s, but also kept the excellent thermal storage capacity by phase transition after no applying current. We further revealed the PGC always kept stable electrical resistance up to 100℃ (Figure S6), demonstrating its high stability and reliability even at overheating conditions. These behaviors provide high practical values of PGC as a dual-functional thermal management system towards more engineering applications.

The key attributes of any storage device are its energy and power characteristics. To quantify the effective energy and power density of our PCM materials in practice, we established a test device as illustrated in Fig. 4a, mainly consisted of an input heat source, thermocouple and PGC material. The thermocouple was put in the center of heater and PGC to detect the temperature change. The mass heat input was rapidly converted into latent heat determined by the thermal conductivity and PGC thickness, and the residual heat was reflected by sensible heat which can cause overheating exceeded the melting point of PCM. Therefore, we think only the storage energy before phase change point was effective energy density in practice (Figure S7). Although the longer time can enable the complete melting of PCM to achieve the totally

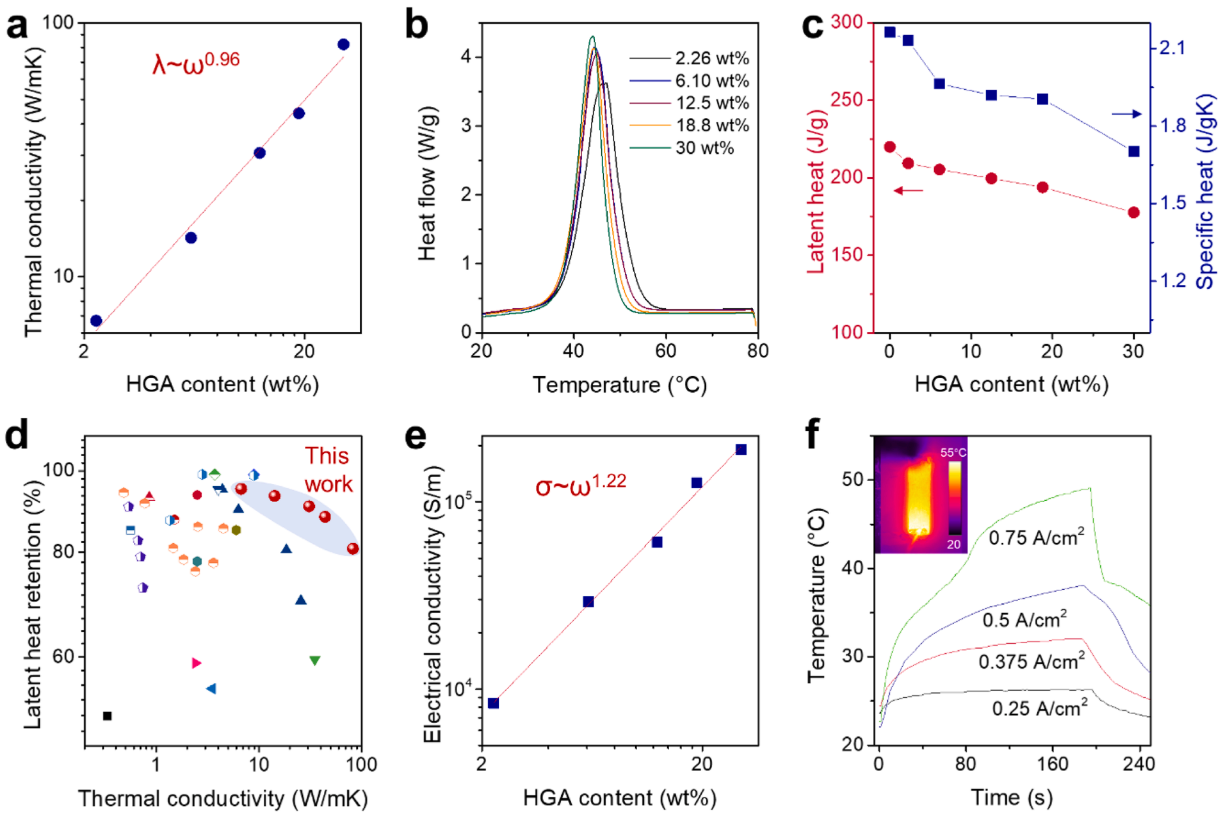

Fig. 3. Thermal and electric heating properties of PGC. **(a)** The relationship between HGA content and thermal conductivity of PGC. **(b)** DSC curves of PGCs with different HGA content. **(c)** The change of latent heat and specific heat of PGC with HGA content. **(d)** A comparison of latent heat retention versus thermal conductivity with previous reported works. **(e)** The relationship between HGA content and electrical conductivity of PGC. **(f)** The temperature rise curves of PGC at different electrical current densities and its thermal imaging at 0.75 A/cm^2.

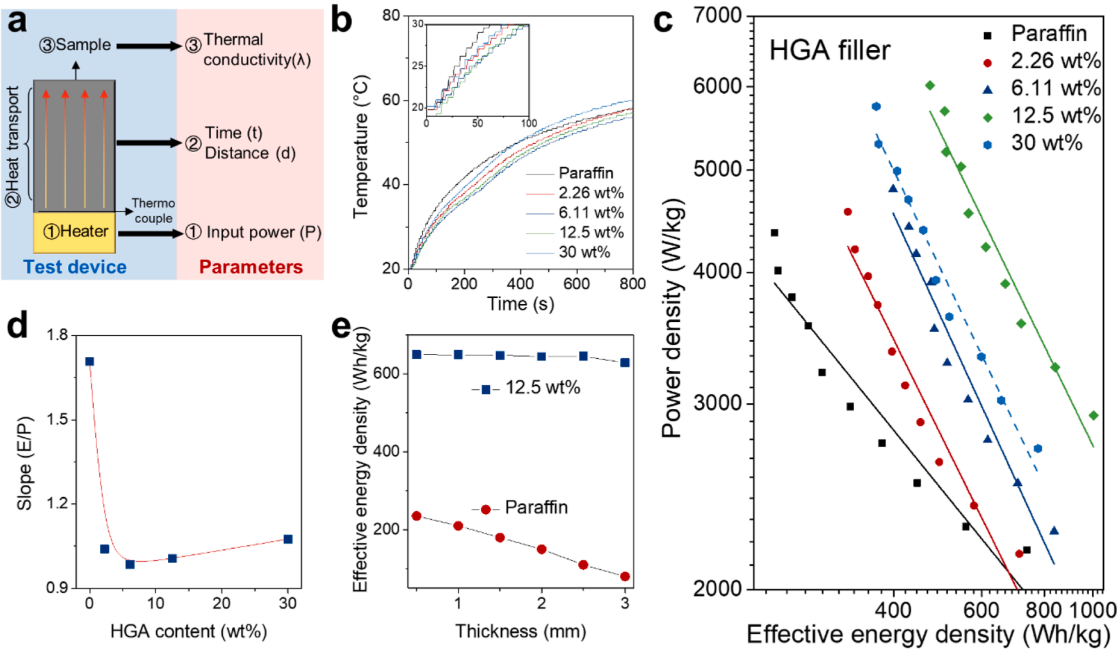

Fig. 4. Effective energy density and power density of PGC. **(a)** A prototype device of effective energy density and power density for PCMs, and their related parameters. **(b)** The temperature increase curves of paraffin and PGCs with an input power of 0.34 W. **(c)** Effective energy density versus power density of paraffin and PGCs. The decrease of effective energy density and power density at 30 wt% marked as dash line. **(d)** The relationship of slope (E/P) and HGA content for PGC. **(e)** The change of effective energy density with thickness for paraffin and PGC with 12.5 wt% HGA filler.

latent heat transformation, the temperature of contact position with heater already exceeded the phase change point or safety window of battery. Only the fast thermal transport in PCM can ensure the total utilization of its intrinsic latent heat as effective energy density, especially in high power density with large heat flux.

As shown in Fig. 4b, there was no obvious plateau region around phase transition point of 42℃ for pure paraffin, indicating the large proportion of input heat was directly converted into sensible heat rather than latent heat, which lost the effectiveness of PCM thermal management. The plateau region of PGCs was prolonged with the increase of graphene loadings before 12.5 wt%, which exhibited the slow tendency of temperature rise at initial stage, inferring the more PCM involved into latent heat conversion. Furthermore, the more graphene fillers in PGC with 30 wt% would reduce the heat storage capacity with shortened platform area because of the low PCM content in composites.

To systematically evaluate the thermal management ability, we perform the measurements of effective energy and power density of PGCs with different HGA filler content (Fig. 4c). We demonstrated the PGCs exhibited the overwhelming superiority than pure paraffin on the effective energy and power density, peaked at the graphene loading of 12.5 wt%. The effective energy density of PGC was up to 1003 Wh/kg, nearly three times more than pure paraffin of 327.7 Wh/kg at power density of 2930 W/kg. Furthermore, the effective energy density of PGC remained about 47.2 % even at power density of 6016.3 W/kg, whereas the pure paraffin only kept 31.3 % at power density of 4362.8 W/kg. The descent rate of effective energy density (*E*) with power density (*P*) was reflected by the slope of E/P, lowered from 1.7 to 1.0 in the filler loading range of 0–12.5 wt% (Fig. 4d), further testifying the high thermal conductivity facilitated the efficient utilization of PCM. Besides, the effective energy density of pure paraffin was dramatically lowered by its thickness (Fig. 4e) because the long distance of heat transport limited the latent heat conversion. As comparison, the effective energy density of PGC with 12.5 wt% HGA was always stable with sample thickness from 0.5 to 3 mm.

3.4. *Thermal management ability for LIBs*

We clarified in detail the practical thermal management ability of PGC for 14,500 LIB cell pack in charging and discharging processes. The maximum capacity of the battery pack in series was 8 Ah. We investigated the temperature changes at different rate capabilities, ranging from 2.75 to 3.75 C, for a battery pack with and without thermal management system using PGC, as the temperature of the battery pack significantly increased under these conditions. The target temperature of bare battery pack was increased rapidly with the charging rate, which was over 100℃ at 3.25 C (Fig. 5a), far beyond the safe temperature window of LIBs. Otherwise, the PGC system significantly suppressed the heat generation during high charging rate, whose temperature only reached ∼ 42℃ at 3.25 C, which was not >60℃ even at 3.75 C. The elevated temperature accelerates irreversible reactions of electrochemical systems, resulting in gas evolution and destruction of structural integrity in the battery, thus increases the internal resistance and overpotential during tests [2]. As shown in Figure S8, the battery pack with thermal management system of PGC exhibited a stable charge-discharge curve at 3–3.5 C, whereas the overpotential of bare battery pack significantly increased during initial period of tests in this situation. Although both of the battery packs exhibited similar overpotentials at 3.75 C, a more serious gas evolution and structural damage can be occurred in the bare battery under this condition. It was induced by variation of electrolyte properties at an extremely high temperature [39], such as viscosity and ionic conductivity, which counteracted the overpotential increased by internal resistance and structural damage of the battery.

The fatigue test of battery is an important parameter to determine the service life [40]. We evaluated the thermal management ability of PGC system at the long-term charging and discharging cycles. At 3 C rate, the temperature of battery pack with PGC system always kept at ∼ 42℃ during the charging and discharging tests for 10,000 cycles, which was lower than the bare battery pack of 64℃ that dissipated heat by thermal convection (Fig. 5b). Owing to the reduction of maximum capacity at high temperature, the battery pack with PGC system needed the more time (∼ 240 h) to realize the cycling tests. Besides, the battery

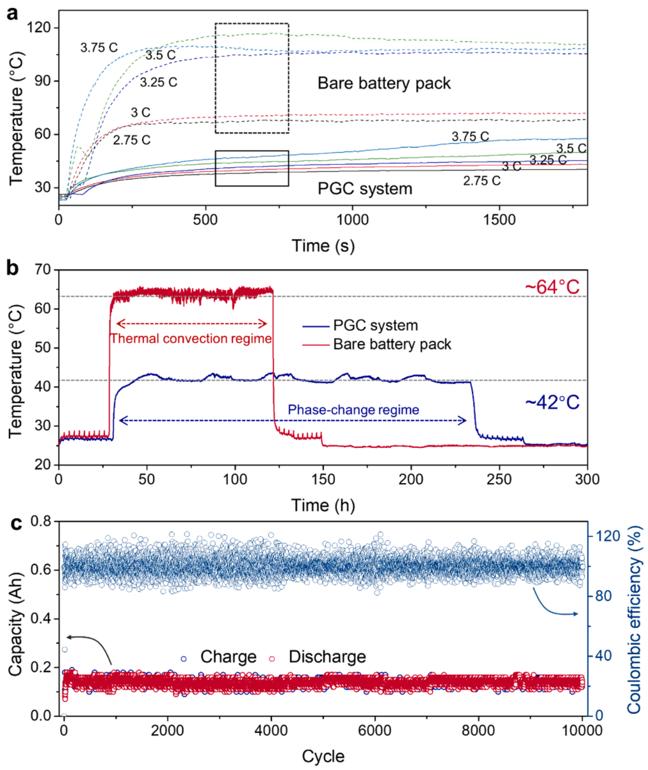

Fig. 5. Thermal management at high-rate charging and discharging of LIB cells. **(a)** The temperature rise curves of bare battery pack and PGC system with capacity rate from 2.75 to 3.75 C. **(b)** The temperature change of bare battery pack and PGC system during 10,000 charging-discharging cycles at 3 C rate. **(c)** The capacity and coulombic efficiency of battery pack with PGC system during 10,000 charging-discharging cycles.

pack with paraffin protection exhibited a narrow phase-change regime because the generated heat cannot be rapidly transport to the whole paraffin monolith (Figure S9). As shown in Fig. 5c and Figure S10, the battery pack with PGC retained 93.3 % capacity after 10,000 cycles at 3 C, benefited from the suppression of undesired electrochemical processes through thermal management. However, the bare battery pack suffered from large joule heat which was not dissipated in time, only retained 63.6 % capacity after the long-term test (Figure S11). Figure S12 given the charge-discharge curve of battery packs at 0.625 before and after above long-term tests to evaluate the battery loss. More serious capacity recession of the bare battery pack was observed compared with the battery pack in PGC on the condition, that both of the battery packs were dissipated joule heat by the air. It indicated that the thermal damage to batteries is an irreversible process. The declined capacity accompanied by dramatic drop can be attributed to decomposition of electrolyte, deteriorated electrode-electrolyte interface, and suddenly structural damage inside battery which exceeded the safe temperature window [41,42].

4. Conclusions

An efficient phase change thermal management system for LIBs protection was developed by hyperbolic graphene-paraffin composite, breaking the trade-off between the high effective energy and power density in conventional PCMs. This is mainly attributed to its superior thermal conductivity (up to ~30.75 W/mK at only 12.5 wt% filler loading), and ultra-high retention ratio of latent heat (~90 %), surpassing most of the reported PCMs. We demonstrate the effective energy density, related to the available latent heat, keeps stable at different applied thicknesses, and is nearly three times more than pure paraffin at same thermal input speed (power density). These outstanding characteristics enable the high efficiency of our PGC to suppress the thermal runaway of LIBs, which realized the reliable and stable operation of 14500 cell pack at 3.75 C rate with working temperature always below 50℃. Even at 10,000 cycles of fast charging and discharge process, the PGC system still enables the safe operation temperature of 42℃, and keeps stable capacity and coulombic efficiency of batteries. We anticipate that this study may pave the way for a simpler and more energy-efficient approach to the thermal management of batteries in a wide range of thermal runaway conditions, which is an important factor for faster adoption of LIB-based energy storage with higher safety.

Financial support

This work is funded by the National Natural Science Foundation of China (Nos. 52090030, 52090031 and 52272046), National Key Research and Development Program of China (2022YFA1205300, 2022YFA1205301), "Pioneer" and "Leading Goose" R&D Program of Zhejiang (2023C01190), the Natural Science Foundation of Zhejiang Province (No. LR23E020003), Hundred Talents Program of Zhejiang University (188020*194231701/113, 112300+1944223R3/003 and 112300+1944223R3/004), the Fundamental Research Funds for the Central Universities (226-2023-00023, 226-2024-00074, 226-2024-00172 and 2023QZJH26), and Shanxi-Zheda Institute of New Materials and Chemical Engineering (Nos. 2022SZ-TD014, 2022SZ-TD011, 2022SZ-TD012).

CRediT authorship contribution statement

Chengqi Zhang: Writing – review & editing, Validation, Methodology, Investigation. **Yi Mao:** Validation, Methodology, Investigation. **Kaiwen Li:** Investigation. **Yingjun Liu:** Supervision, Project administration, Funding acquisition. **Zhen Xu:** Writing – review & editing, Supervision, Resources, Project administration, Funding acquisition, Conceptualization. **Kai Pang:** Writing – review & editing, Writing – original draft, Validation, Methodology, Investigation, Formal analysis, Conceptualization. **Shengying Cai:** Writing – review & editing, Supervision, Resources, Methodology, Investigation, Conceptualization. **Liwu Fan:** Writing – review & editing, Formal analysis. **Chao Gao:** Writing – review & editing, Validation, Supervision, Resources, Project administration, Methodology, Funding acquisition, Conceptualization.

Declaration of competing interest

The authors declare that they have no known competing financial interests or personal relationships that could have appeared to influence the work reported in this paper.

Supplementary materials

Supplementary material associated with this article can be found, in the online version, at doi:10.1016/j.ensm.2025.104003.

Data availability

Data will be made available on request.

References

[1] J.M. Tarascon, M. Armand, Issues and challenges facing rechargeable lithium batteries, Nature 414 (2001) 359–367, https://doi.org/10.1038/35104644.

[2] M.T.F. Rodrigues, G. Babu, H. Gullapalli, K. Kalaga, F.N. Sayed, K. Kato, J. Joyner, P.M. Ajayan, A materials perspective on Li-ion batteries at extreme temperatures, Nat. Energy. 2 (2017) 1–14, https://doi.org/10.1038/nenergy.2017.108.

[3] D. Deng, Li-ion batteries: basics, progress, and challenges, Energ. Sci. Eng. 3 (2015) 385–418, https://doi.org/10.1002/ese3.95.

[4] T. Bandhauer, S. Garimella, T. Fuller, A critical review of thermal issues in lithium-ion batteries, J. Electrochem. Soc. 158 (2011) 1–25, https://doi.org/10.1149/1.3515880.

[5] Q. Wang, B. Jiang, B. Li, Y. Yan, A critical review of thermal management models and solutions of lithium-ion batteries for the development of pure electric vehicles, Renew. Sust. Energ. Rev. 64 (2016) 106–128, https://doi.org/10.1016/j.rser.2016.05.033.

[6] Z.G. Shen, S. Chen, X. Liu, B. Chen, A review on thermal management performance enhancement of phase change materials for vehicle lithium-ion batteries, Renew. Sust. Energ. Rev. 148 (2021) 111301, https://doi.org/10.1016/j.rser.2021.111301.

[7] J. Woods, A. Mahvi, A. Goyal, E. Kozubal, A. Odukomaiya, R. Jackson, Rate capability and Ragone plots for phase change thermal energy storage, Nat. Energy. 6 (2021) 295–302, https://doi.org/10.1038/s41560-021-00778-w.

[8] R.A. Lawag, H.M. Ali, Phase change materials for thermal management and energy storage: a review, J. Energy Storage. 55 (2022) 105602, https://doi.org/10.1016/j.est.2022.105602.

[9] P. Cheng, X. Chen, H. Gao, X. Zhang, Z. Tang, A.G. Wang, Different dimensional nanoadditives for thermal conductivity enhancement of phase change materials: fundamentals and applications, Nano Energy 85 (2021) 105948, https://doi.org/10.1016/j.nanoen.2021.105948.

[10] H. Ji, D.P. Sellan, M.T. Pettes, X. Kong, J. Ji, L. Shi, R.S. Ruoff, Enhanced thermal conductivity of phase change materials with ultrathin-graphite foams for thermal energy storage, Environ. Sci. 7 (2014) 1185–1192, https://doi.org/10.1039/C3EE42573H.

[11] M. Wu, T. Li, Q. He, R. Du, R. Wang, Thermally conductive and form-stable phase change composite for building thermal management, Energy 239 (2022) 121938, https://doi.org/10.1016/j.energy.2021.121938.

[12] S. Wu, T. Li, Z. Tong, J. Chao, T. Zhai, J. Xu, T. Yan, M. Wu, Z. Xu, H. Bao, T. Deng, R. Wang, High-performance thermally conductive phase change composites by large-size oriented graphite sheets for scalable thermal energy harvesting, Adv. Mater. 31 (2019) 1905099, https://doi.org/10.1002/adma.201905099.

[13] X. Feng, M. Ouyang, X. Liu, L. Lu, Y. Xia, X. He, Thermal runaway mechanism of lithium ion battery for electric vehicles: a review, Energy Storage Mater 10 (2018) 246–267, https://doi.org/10.1016/j.ensm.2017.05.013.

[14] L. Ma, M. Nie, J. Xia, J.R. Dahn, A systematic study on the reactivity of different grades of charged $Li[Ni_xMn_yCo_z]O_2$ with electrolyte at elevated temperatures using accelerating rate calorimetry, J. Power Sources. 327 (2016) 145–150, https://doi.org/10.1016/j.jpowsour.2016.07.039.

[15] K. Pang, X. Song, Z. Xu, X. Liu, Y. Liu, L. Zhong, Y. Peng, J. Wang, J. Zhou, F. Meng, J. Wang, C. Gao, Hydroplastic foaming of graphene aerogels and artificially intelligent tactile sensors, Sci. Adv. 6 (2020) eabd4045, https://doi.org/10.1126/sciadv.abd4045.

[16] X. Liu, K. Pang, H. Qin, Y. Liu, Y. Liu, C. Gao, Z. Xu, Hyperbolic graphene framework with optimum efficiency for conductive composites, ACS Nano 16 (2022) 14703–14712, https://doi.org/10.1021/acsnano.2c05414.

[17] Y. Chen, K. Pang, X. Liu, K. Li, J. Lu, S. Cai, Y. Liu, Z. Xu, C. Gao, Environment-adaptive, anti-fatigue thermal interface graphene foam, Carbon N Y 212 (2023) 118142, https://doi.org/10.1016/j.carbon.2023.118142.

[18] L. Peng, Z. Xu, Z. Liu, Y. Guo, P. Li, C. Gao, Ultrahigh thermal conductive yet superflexible graphene films, Adv. Mater. 29 (2017) 1700589, https://doi.org/10.1002/adma.201700589.

[19] L. Peng, Y. Han, M. Wang, X. Cao, J. Gao, Y. Liu, X. Chen, B. Wang, B. Wang, C. Zhu, X. Wang, K. Cao, M. Huang, B.V. Cunning, J. Pang, W. Xu, Y. Ying, Z. Xu, W. Fang, Y. Lu, R.S. Ruoff, C. Gao, Multifunctional macroassembled graphene nanofilms with high crystallinity, Adv Mater 33 (2021) 2104195, https://doi.org/10.1002/adma.202104195.

[20] Y. Wang, B. Tang, S. Zhang, Single-walled carbon nanotube/phase change material composites: sunlight-driven, reversible, form-stable phase transitions for solar thermal energy storage, Adv. Funct. Mater. 23 (2013) 4354–4360, https://doi.org/10.1002/adfm.201203728.

[21] G. Li, X. Zhang, J. Wang, J. Fang, From anisotropic graphene aerogels to electron- and photo-driven phase change composites, J. Mater. Chem. A. 4 (2016) 17042–17049, https://doi.org/10.1039/C6TA07587H.

[22] P. Min, J. Liu, X. Li, F. An, P. Liu, Y. Shen, N. Koratkar, Z.Z. Yu, Thermally conductive phase change composites featuring anisotropic graphene aerogels for real-time and fast-charging solar-thermal energy conversion, Adv. Funct. Mater. 28 (2018) 1805365, https://doi.org/10.1002/adfm.201805365.

[23] H.Y. Zhao, M.Y. Yu, J. Liu, X. Li, P. Min, Z.Z. Yu, Efficient preconstruction of three-dimensional graphene networks for thermally conductive polymer composites, Nano-Micro Lett 14 (2022) 129, https://doi.org/10.1007/s40820-022-00878-6.

[24] W. Dai, L. Lv, T. Ma, X. Wang, J. Ying, Q. Yan, X. Tan, J. Gao, C. Xue, J. Yu, Y. Yao, Q. Wei, R. Sun, Y. Wang, T.H. Liu, T. Chen, R. Xiang, N. Jiang, Q. Xue, C.P. Wong, S. Maruyama, C.T. Lin, Multiscale Structural modulation of anisotropic graphene framework for polymer pomposites achieving highly efficient thermal energy management, Adv. Sci. 8 (2021) 2003734, https://doi.org/10.1002/advs.202003734.

[25] P. Liu, X. Liu, P. Min, X. Chang, C. Shu, Y. Ding, Z.Z. Yu, 3D lamellar-structured graphene aerogels for thermal interface composites with high through-plane thermal conductivity and fracture toughness, Nano-Micro Lett 13 (2021) 22, https://doi.org/10.1007/s40820-020-00548-5.

[26] J. Ying, X. Tan, L. Lv, X. Wang, J. Gao, Q. Yan, H. Ma, K. Nishimura, H. Li, J. Yu, T. H. Liu, R. Xiang, R. Sun, N. Jiang, C. Wong, S. Maruyama, C.T. Lin, W. Dai, Tailoring highly ordered graphene framework in epoxy for high-performance polymer-based heat dissipation plates, ACS Nano 15 (2021) 12922–12934, https://doi.org/10.1021/acsnano.1c01332.

[27] J. Yang, E. Zhang, X. Li, Y. Zhang, J. Qu, Z.Z. Yu, Cellulose/graphene aerogel supported phase change composites with high thermal conductivity and good shape stability for thermal energy storage, Carbon N Y 98 (2016) 50–57, https://doi.org/10.1016/j.carbon.2015.10.082.

[28] W. Aftab, A. Mahmood, W. Guo, M. Yousaf, H. Tabassum, X. Huang, Z. Liang, A. Cao, R. Zou, Polyurethane-based flexible and conductive phase change composites for energy conversion and storage, Energy Storage Mater 20 (2019) 401–409, https://doi.org/10.1016/j.ensm.2018.10.014.

[29] N. Sheng, R. Zhu, L. Dong, T. Nomura, C. Zhu, Y. Aoki, H. Habazaki, T. Akiyama, Vertically aligned carbon fibers as supporting scaffolds for phase change composites with anisotropic thermal conductivity and good shape stability, J. Mater. Chem. A. 7 (2019) 4934–4940, https://doi.org/10.1039/C8TA11329G.

[30] Y. Xia, H. Zhang, P. Huang, C. Huang, F. Xu, Y. Zou, H. Chu, E. Yan, L. Sun, Graphene-oxide-induced lamellar structures used to fabricate novel composite solid-solid phase change materials for thermal energy storage, Chem. Eng. J. 362 (2019) 909–920, https://doi.org/10.1016/j.cej.2019.01.097.

[31] J. Yang, L.S. Tang, R.Y. Bao, L. Bai, Z.Y. Liu, W. Yang, B.H. Xie, M.B. Yang, An ice-templated assembly strategy to construct graphene oxide/boron nitride hybrid porous scaffolds in phase change materials with enhanced thermal conductivity and shape stability for light–thermal–electric energy conversion, J. Mater. Chem. A. 4 (2016) 18841–18851, https://doi.org/10.1039/C6TA08454K.

[32] D. Li, X. Cheng, Y. Li, H. Zou, G. Yu, G. Li, Y. Huang, Effect of MOF derived hierarchical Co3O4/expanded graphite on thermal performance of stearic acid phase change material, Sol. Energy. 171 (2018) 142–149, https://doi.org/10.1016/j.solener.2018.06.062.

[33] Y. Zhao, X. Min, Z. Huang, Y. Liu, X. Wu, M. Fang, Honeycomb-like structured biological porous carbon encapsulating PEG: a shape-stable phase change material with enhanced thermal conductivity for thermal energy storage, Energ. Buildings. 158 (2018) 1049–1062, https://doi.org/10.1016/j.enbuild.2017.10.078.

[34] H. Tabassum, X. Huang, R. Chen, R. Zou, Tailoring thermal properties via synergistic effect in a multifunctional phase change composite based on methyl stearate, J. Materiomics. 1 (2015) 229–235, https://doi.org/10.1016/j.jmat.2015.07.002.

[35] R. Akula, C. Balaji, Thermal management of 18650 Li-ion battery using novel fins-PCM-EG composite heat sinks, Appl. Energy. 316 (2022) 119048, https://doi.org/10.1016/j.apenergy.2022.119048.

[36] A.R.M. Siddique, S. Mahmud, B.V. Heyst, A comprehensive review on a passive (phase change materials) and an active (thermoelectric cooler) battery thermal management system and their limitations, J. Power Sources. 401 (2018) 224–237, https://doi.org/10.1016/j.jpowsour.2018.08.094.

[37] T. Li, M. Wu, S. Wu, S. Xiang, J. Xu, J. Chao, T. Yan, T. Deng, R. Wang, Highly conductive phase change composites enabled by vertically-aligned reticulated graphite nanoplatelets for high-temperature solar photo/electro-thermal energy conversion, harvesting and storage, Nano Energy 89 (2021) 106338, https://doi.org/10.1016/j.nanoen.2021.106338.

[38] R. Zheng, J. Gao, J. Wang, G. Chen, Reversible temperature regulation of electrical and thermal conductivity using liquid–solid phase transitions, Nat. Commun. 2 (2011) 289, https://doi.org/10.1038/ncomms1288.

[39] J. Landesfeind, H.A. Gasteiger, Temperature and concentration dependence of the ionic transport properties of lithium-ion battery electrolytes, J. Electrochem. Soc. 166 (2019) 3079–3097, https://doi.org/10.1149/2.0571912jes.

[40] J. Porzio, C.D. Scown, Life-cycle assessment considerations for batteries and battery materials, Adv. Energy Mater. 11 (2021) 2100771, https://doi.org/10.1002/aenm.202100771.

[41] J. Deng, C. Bae, J. Marcicki, A. Masias, T. Miller, Safety modelling and testing of lithium-ion batteries in electrified vehicles, Nat. Energy. 3 (2018) 261–266, https://doi.org/10.1038/s41560-018-0122-3.

[42] M. Kaliaperumal, M.S. Dharanendrakumar, S. Prasanna, K.V. Abhishek, R. K. Chidambaram, S. Adams, K. Zaghib, M.V. Reddy, Cause and mitigation of lithium-ion battery failure—A review, Materials (Basel) 14 (2021) 5676, https://doi.org/10.3390/ma14195676.